Role of sintering temperature dependent crystallization of bioactive glasses on erythrocyte and cytocompatibility

Shivalingam Chitra[1], Purushothaman Bargavi[1], Dhinasekaran Durgalakshmi[2], Padmanaban Rajashree[3], Subramanian Balakumar[1,*]

[1]*National Centre for Nanoscience and Nanotechnology University of Madras, Guindy Campus, Chennai-600025, India*
[2]*Department of Medical Physics, Anna University, Chennai-600025, India*
[3]*Centre for Advanced Study in Crystallography and Biophysics University of Madras, Guindy Campus, Chennai-600025, India*

Abstract

Bioglass (BG) was prepared by sol-gel method and the role of sintering temperatures (600, 700 and 800 °C) on crystalline phase changes, bioactivity, erythrocyte and MG-63 cell line compatibility was investigated. Increase in sintering temperature from 600 to 800 °C led to the secondary phase formation that was confirmed through structural analysis. Micrographics revealed the formation of nanorods (700 °C) and nanoflake like (800 °C) morphologies. Biocompatibility assay showed that, BG sintered at 600 °C had optimal biocompatibility while better mechanical property was noted at 700 °C. Altogether, the study demonstrated that increasing the sintering temperature will result in increased crystallinity which in turn resulted in the optimal biomineralization but decreased the biocompatibility. Hence, we demonstrated the importance of temperature during the processing of BG for various applications, as it affects many properties including bioactivity and compatibility.

Keywords: bioactive glass, sol-gel, sintering, bioactivity, biocompatibility

I. Introduction

The Bioglass 45S5 particulates have been used in the name of NovaBone® (NovaBone products LLC, Jacksonville, FL) [1] to cure maxillofacial and orthopaedic defects. The Endosseous Ridge Maintenance Implant (ERMI) introduced a bioglass (BG) into the tooth extracted sites in the form of cone and putty as implants [2]. PerioGlas (US Biomaterials at present sold to NovaBone) was used to treat periodontal diseases [3]. Biogran is one of other forms of the Bioglass 45S5 (Biomet 3i, palm Beach Gardens, FL) which is used for jaw bone defects [4]. The current issue is that in all the commercial materials particle sizes are greater than 50 µm, which may cause the toxicity at the genomic level [5]. Hence with the advent of nanotechnology, the research has moved towards optimisation of crystallinity and morphological characteristic features, to gain better bioactive as well as biocompatible materials. Even though several varieties of commercial materials have evolved; still research is needed to improve the aspect of dissolution/degradation resulting from the bioactivity/biocompatibility.

The advantage of bioglass is its easy bonding with both bone and tissue [6,7] and faster response and interaction between implant material and host tissue than other biomaterials such as hydroxyapatite and tricalcium phosphate [8]. However, several processing routes, such as the production of scaffolds or the deposition of coatings, include a thermal treatment to apply or sinter the glass. The exposure to high temperature may induce a devitrification phenomenon, altering the properties and, in particular, the bioactivity of the glass. During sintering, the material becomes more compact, whereas the degree of porosity decreases and interconnecting porosity may be lost. Thus, osteoconductivity will be reduced and biodegradability becomes more difficult [9]. Often, ceramic particles are still visible, even after sev-

*Corresponding author: tel: +44 22202749,
e-mail: *balasuga@yahoo.com*

eral years. They have a negative influence on the mechanical properties of the bone and favour chronic inflammation [10].

The bioglass 45S5 system contains 45 wt.% of SiO_2, 24.5 wt.% Na_2O, 24.5 wt.% CaO and 6 wt.% of P_2O_5 and mostly two methods are used for the synthesis: melt quenching and sol-gel method. We used the sol-gel method to prepare bioglass, because this technique takes lower preparation temperature, better control, good quality, minimal cost and produces BG with high surface area accelerating the rate of hydroxyapatite formation [11,12]. It is evident from the literature that mechanical stability increases with increase in crystallinity [13]. Massera *et al.* [14] studied BG crystallization mechanism and its structural properties and reported that better bioactivity results as a consequence of partial crystallisation. Furthermore, Thomas *et al.* [15] expressed that crystallization mechanism depends on sintering kinetics which contributes to the understanding of the structural behaviour and phase transition in BG. Thus, as it is shown in Table 1 a few reports are available on the structure stabilisation of BG at various temperatures, however the relation between biocompatibility and crystallization temperature are sparsely reported. Hence, we intend are intended to bring out the significance of various sintering temperatures on the erythrocyte compatibility, ALP activity, and cytocompatibility in addition to bio mineralization of BG.

II. Experimental procedure

2.1. Materials and methods

All the chemicals and reagents used in the present work are analytical grade without additional purification. TEOS (tetraethyl orthosilicate (98% pure) was purchased from Alfa Aesar, orthophosphoric acid (88% pure), calcium nitrate (99% pure) and nitric acid (70% pure) were purchased from Spectrum Reagents and Chemicals Pvt. Ltd., sodium hydroxide (98% pure) was purchased from Sisco research laboratory. These chemicals were utilized to prepare bioglass, through sol-gel method. Firstly, 45% of TEOS (tetraethyl orthosilicates) was added with double distilled water, nitric acid and ethanol for silica hydrolysis. It was stirred for 1 h to form a complete gel. Then reagents were dissolved individually for 45 min and added to silica matrix in the following order and amount: 6% orthophosphoric acid, 24.5% calcium nitrate and finally sodium hydroxide 24.5%. The resultant product was a white sol that was kept for ageing under stirring for 12 h to form a highly ordered gel matrix and then it was dried in a hot air oven for 24 h at 120 °C. Finally, in order to stabilize the phase formation, heat treatment was adopted at different temperatures such as 600, 700 and 800 °C for 3 h in a box furnace under ambient atmosphere. Thereafter, they will be designated as BG600, BG700 and BG800, respectively.

Table 1. Literature survey of bioglass crystallinity with respect to biocompatibility

Method of synthesis	Crystalline phase and sintering temperature	Biocompatibility/ Bioactivity	Ref.
Bioglass® powder by melt quenching method	$Na_2CaSi_2O_6$ – 800 °C $Na_2Ca_4(PO_4)_2SiO_4$ – 800 to 950 °C	Assessed biodegradation in the terms of preferential dissolution	[16]
Bioglass® structural transformations reported by melt quenching method	$Na_2CaSi_2O_6$ – 600 to 750 °C	–	[17]
Bioglass® (45S5) powder from NovaMin USA	$Na_2Ca_2Si_3O_9$ – 1050 °C for 140 min	–	[18]
Bioglass prepared by sol-gel process	Wollastonite, apatite and pseudo wollastonite phases – 1000 °C	Elevated *in vitro* apatite formation at 1000 °C	[19]
45S5 bioglass purchased by U.S. Biomaterials Corp. and ball milled for 4 h	$Na_2Ca_2Si_3O_9$ – 1000 °C	Wollastonite phase was formed after mineralization	[20]
Bioglass synthesised by sol-gel method	$Na_2CaSi_2O_6$, $Ca_5(PO_4)_2SiO_4$, $CaSiO_3$ – 700 to 1000 °C Wollastonite phase – 1100 °C	*In vitro* dissolution kinetics was found in the presence of crystalline phase	[21]
Bioglass® powder using spark plasma sintering	Amorphous – 550 °C $Na_2CaSi_2O_6$ – 600 °C	BG (600 °C) showed improved bioactivity	[22]
Melt derived 45S5 powder sintered by spark plasma sintering (SPS)	$Na_2CaSi_3O_8$ – 500 to 600 °C	Investigated cell proliferation and alkaline phosphatase activity by MG-63 and L929 cell line	[23]

2.2. Material characterization

The prepared bioglass was characterized to study its thermal properties using thermogravimetric analysis and differential thermal analysis (SII Nanotechnology-TG/DTA-6300, Japan). Structural and phase conformations were examined using X-ray diffraction (XRD, PANalytical Instruments, The Netherlands) using Cu-$K\alpha_1$ radiation ($\lambda = 0.154$ nm) with the scanning rate of $2\theta = 3°$/min. The morphological changes of BG before and after immersion were examined using field emission scanning electron microscope (FESEM, HI-TACHI SU-6600, Japan) with the electron beam energy of 15 keV. Further on, to confirm the molecular vibrations, we utilized Raman and Fourier transform infrared spectroscopy (Nanophoton Raman 11i, Japan and Perkin Elmer Spectrum-1). Vickers hardness test was carried out according to C 1327-03 ASTM standard by Vickers microhardness tester Wilson Wolpert, Germany with the load of 0.98 N. Biocompatibility properties were analysed by haemolytic assay with erythrocytes and cell proliferation assay using MG-63 (osteosarcoma) cell line. Apparent porosity was estimated using Archimedes technique as reported by Seyedmajidi *et al.* [24]. All the three sintered and as-prepared bioglass pellets (50 mg samples were used to make pellets by pelletizer with 80 bar pressure) were immersed in boiling water for 3 h. Dry weight, suspended weight and saturated weight of the bioglass pellets were measured before and after immersion to determine the porosity of the samples. Subsequently apparent porosities (P) of the pellets were calculated using the formula (1):

$$P = \frac{SaW - DW}{SaW - SuW} \cdot 100 \qquad (1)$$

where SaW is saturated weight, DW is dry weight and SuW is suspended weight.

2.3. In vitro bioactivity test

In vitro bioactivity of the sample was investigated using simulated body fluid (SBF). SBF has the ionic composition nearly similar to human blood plasma. Bone bonding ability of the bioglass samples was essentially assessed using SBF. The powder samples (100 mg) were made into 8 mm pellet by pelletizer with the pressure up to 80 bar. Then, BG samples were immersed in SBF solution for an appropriate duration to analyse the formation of hydroxyapatite (HA) or hydroxyl carbonate apatite (HCA) layer on the surface of bioglass. The reaction between SBF and bioglass is similar to bioglass reacting with body fluid [25,26]. HCA layer formation occurs on the surface of the material, which will initiate the osteo-production. The bioglass pellets were immersed in 10 ml of SBF at the temperature of 37 °C. In the present study, the immersion was carried out for 7 days. As a final point, the samples were filtered using Whatmann filter paper and dried in the hot air oven at 70 °C for 5 h. To investigate the apatite formation we used FESEM to examine the morphological changes due to gradual dissolution and the formation of bone like hydroxyl carbonate apatite layer on the material surface.

2.4. Haemocompatibility studies

Haemocompatibility is one of the essential methods to evaluate the compatibility of any biomaterial using erythrocytes. Initially, blood was collected from volunteer donor retained by using EDTA to inhibit the coagulation and centrifuged for 10 min at 4 °C, and again washed 2 to 3 times using phosphate buffer saline (PBS) to separate plasma. The obtained blood sample (50 µl) and PBS (950 µl) were mixed with bioglass samples in Eppendorf tubes. All bioglass samples were analysed in triplicates ($n = 3$) with varying concentration, such as 0.5 mg/ml, 1 mg/ml, and 2.5 mg/ml, and further incubated for 1 h at 37 °C. Then the samples were centrifuged for 10 min at 4 °C and the optical density value was noted at 540 nm. The haemolysis (H) was calculated using the formula (2):

$$H = \frac{SA - NC}{PC - NC} \cdot 100 \qquad (2)$$

where SA is sample absorbance, NC is negative control and PC is positive control.

2.5. Cytocompatibility studies

MG-63 cell line is commonly employed cell line to analyse the compatibility of biomaterial with bone and to see its effect on the cells proliferation. The biocompatibility of the bioglass sintered at various temperatures was evaluated using MTT (methyl thiazolyl-diphenyl-tetrazolium bromide) assay. The cells were maintained in Dulbecco's Modified Eagle's Medium (DMEM) supplemented with 10% fetal bovine serum (FBS) and 1% antibiotics (tetracycline). The cells (1×10^5/well) were plated in 96-well plate and incubated at 37 °C with 5% CO_2 atmosphere. Various concentrations (100, 75, 50, 25, and 10 µg/µl) of the samples were added and incubated for 24, 48 and 72 h, respectively. After specific incubation duration, the medium was removed from the well and washed with phosphate buffered saline (pH 7.4). Methyl thiazolyl-diphenyl-tetrazolium bromide was added to the samples at 50 µl/well (5 mg/ml) of 0.5% MTT and incubated for 4 h. After incubation, 100 µl of DMSO (dimethyl sulfoxide) was added to all the wells to solubilize the formazan crystals, formed after the reaction between mitochondrial dehydrogenase and MTT. The optical density at 570 nm was measured by ELISA reader. Cell viability (CV) was calculated using the following formula (3):

$$CV = \frac{SA}{SC} \cdot 100 \qquad (3)$$

where SA is sample absorbance and SC is sample control.

III. Results and discussion

3.1. Thermogravimetric analysis

Thermogravimetric analysis was used to measure the change in mass of BG with respect to temperature up to 1000 °C. TGA curve (Fig. 1) shows total of 42.7% weight loss in two stages. In the first stage, 16% weight loss occurred from 29 to 148 °C due to the removal of water and −OH groups [16]. In the second stage, 26% weight loss was observed from 573 to 781 °C, initiating the crystallization in BG. Accordingly the endothermic peak of the DTA spectra reflects the removal of alcohol and physically adsorbed water molecules. The exothermic peak centred at 300 °C is attributed to the removal of nitrate groups [27]. The second endothermic peak at 732 °C might represent the melting point of crystalline phase, and above 800 °C starts secondary phase formation that can be further confirmed from XRD analysis [17,28]. Thus, from the above analysis it is found that the onset of phase transition in BG occurs at 732 °C. We chose 3 sintering temperatures, 600, 700 and 800 °C respectively to evaluate the *in vitro* biomineralization ability and biocompatibility with respect to crystallinity.
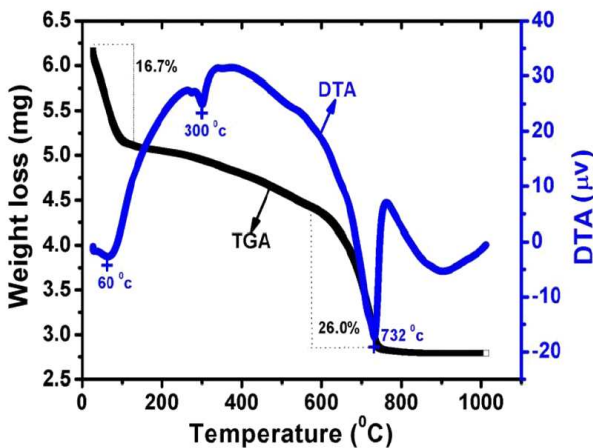

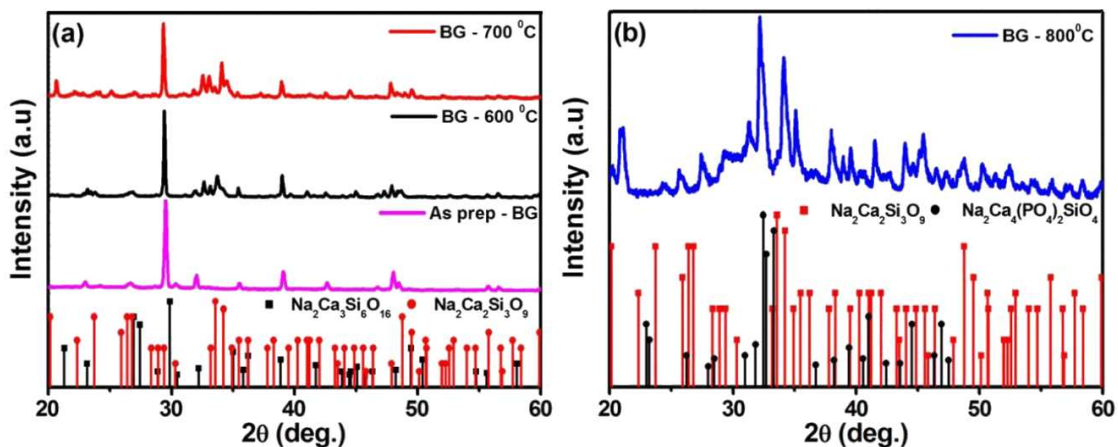**Figure 1. TGA and DTA analysis of Bioglass representing broad thermal variations**

3.2. Structural analysis

The BG samples were subjected to XRD analysis to study the phase and crystalline structure of sodium calcium silicate system. In general, BG is amorphous in nature; however, the pattern shows crystallinity due to the incorporation of sodium into the bioglass system [29]. The XRD pattern corresponding to BG600 and BG700 are shown in (Fig. 2). They match well with dual phases of $Na_2Ca_3Si_6O_{16}$ (JCPDS No. 23-0671) with anorthic structure and $Na_2Ca_2Si_3O_9$ (JCPDS No. 22-1455) with hexagonal crystal system. Contrarily, in BG800, new small peaks were observed and differences were noted in relative intensity peaks, which may be due to the different crystal orientation of BG800. This indicates a phase transition to $Na_2Ca_4(PO_4)_2SiO_4$ crystalline phase (JCPDS No-32-1053).

It can be seen that the sodium-related peak is the maximum intense peak in BG600 and BG700, whereas in BG800, sodium peak gets suppressed and calcium phosphate peak intensity seemed to be enhanced. Current XRD spectra denotes the $Na_2Ca_4(PO_4)_2SiO_4$ (silicorhenanite) as a major phase in BG800. Lattice arrangements may vary by increasing the sintering temperature; hence crystal structure and phases can also be modified. Lefebvre *et al.* [30] reported that dual oxygen-phosphorus bond can create a platform for the formation of phosphate phase on the silica network which increases the crystallization. Our study clearly depicts that, by increasing the sintering temperature, crystallinity of sodium calcium silicate phase was increased with the phase transition to $Na_2Ca_4(PO_4)_2SiO_4$.

3.3. Raman and FTIR

The Raman spectra of the as-prepared BG, BG600, BG700 and BG800 are shown in (Fig. 3a). It is found that the peaks at 965, 966 and 967 cm⁻¹ representing P−O−P symmetric stretching indicate the presence of phosphate in all the samples. Also peaks at 1066 cm⁻¹ and 1020 cm⁻¹ represent Q^4 Si−O−Si symmetric stretching in all BG samples. The shoulder peak that appears around 939 cm⁻¹ in the spectra of BG700

Figure 2. XRD pattern of: a) as-prepared BG, BG600, BG700 and b) BG800 samples
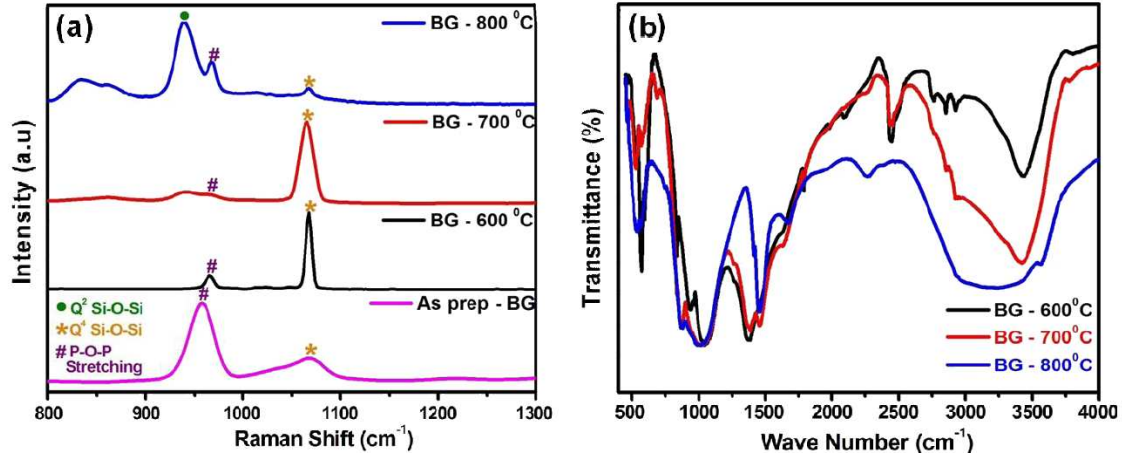
Figure 3. Raman spectra (a) and FTIR spectral analysis (b) of bioglass samples sintered at different temperatures

is found to develop when the temperature is raised to 800 °C and denotes Q^2 Si−O−Si stretching in BG800. These results are consistent with that of the XRD confirming the phase transition between 700 and 800 °C resulting in a phase with phosphate as one of the components. Additionally, silica peak present at 1066 cm^{-1} is gradually suppressed as the temperature increases that could be due to the formation of secondary phase.

FTIR spectra of BG600 to BG800 are shown in (Fig. 3b). BG600 transmission spectra denote the peak centred at 573 cm^{-1} ascribed to P−O bending vibrations of apatite-like calcium phosphate phase [29]. The peaks centred at 1044 and 934 cm^{-1} are attributed to Si−O−Si tetrahedral and Si−O−Si stretching modes, respectively. BG700 shows P−O crystalline bending at 533 cm^{-1}. Similarly, a P−O bending vibration was observed at 570 and 558 cm^{-1}. The peaks that are present in the re-

gions of 865 and 1021 cm^{-1} are attributed to carbonate group and Si−O−Si tetrahedral vibrations respectively. The BG800 indicates the Si−O−Si bending, carbonate group and Si−O−Si tetrahedral vibrational modes, observed at 541, 879 and 1015 cm^{-1}. The peaks present near 568 cm^{-1} are attributed to P−O bending mode. Si−O−Si bending and carbonate groups were observed in the range of 835 and 1400 cm^{-1}. The spectral signatures of Raman and FTIR spectra of the bioglass system with respect to the earlier literature are reported in Table 2.

3.4. Morphological analysis

The surface morphology and homogeneity of BG samples, as-prepared and sintered at various temperatures, were imaged using FESEM and are displayed in Fig. 4. The morphology and particle size distribution of

Table 2. Raman and FTIR peak positions and the functional group assignments

Raman peak position [cm^{-1}]	Assignment	References
965, 966, 967	P–O–P symmetric stretching	[31–33]
1066, 1020	Q^4 Si–O–Si symmetric stretching	[33–35]
939	Q^2 Si–O–Si stretching	[36]

| FTIR peak positions [cm^{-1}]	Assignment	References
573	P–O bending	[29,31]
1044	Si–O–Si tetrahedral	[37]
934	Si–O–Si stretching	[13, 37]
533	P–O crystalline bending	[37]
570, 558	P–O bending	[38,39]
865	Carbonate group	[40]
1021	Si–O–Si tetrahedra	[41]
541	Si–O–Si bending	[37]
879	Carbonate group	[13,40]
1015	Si–O–Si tetrahedral	[41]
568	P–O bending	[42]
835	Si–O–Si bending	[33]
1400	Carbonate group	[39]
3000–3750	H$_2$O stretchings	[43]
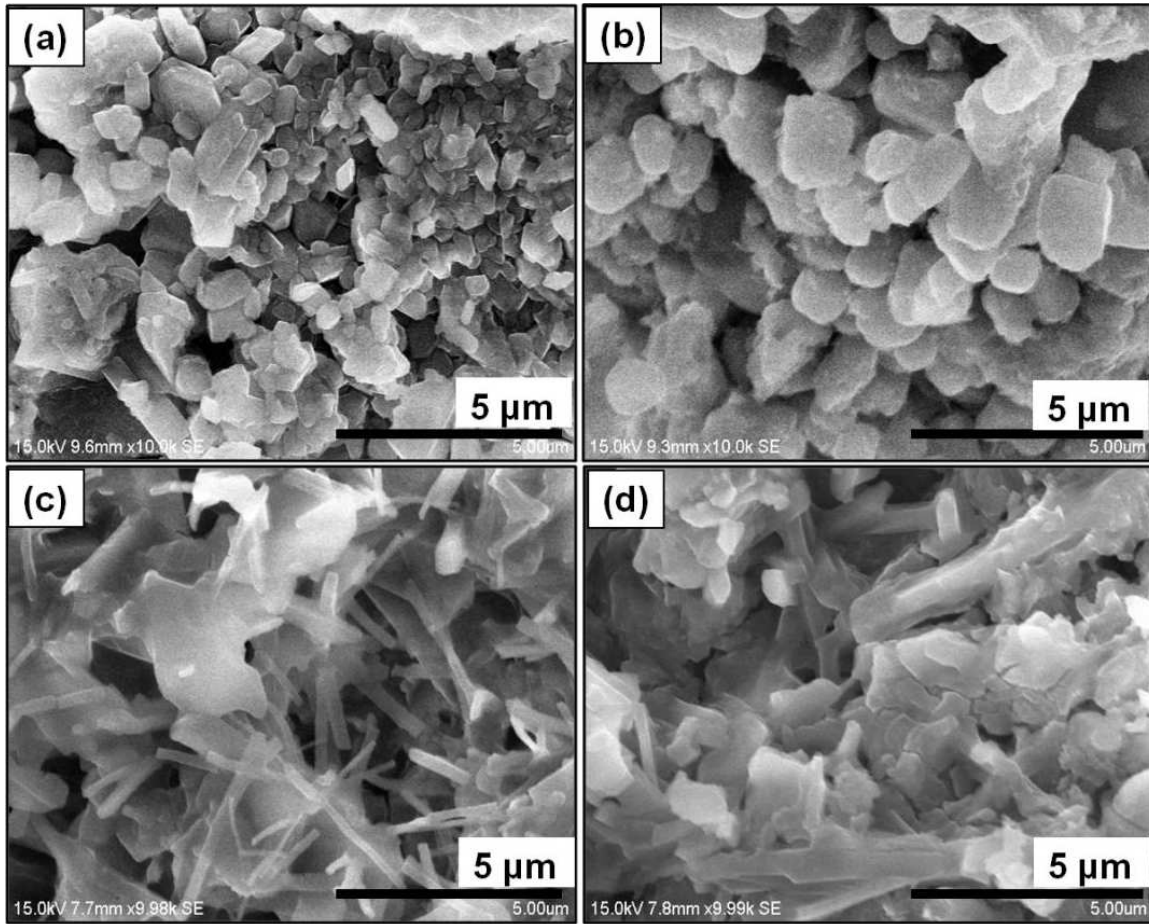
Figure 4. FESEM analysis of: a) as-prepared BG, b) BG600, c) BG700 and d) BG800 samples

BG is found to vary when the temperature was gradually increased. From Fig. 4a the micrographs corresponding to the as-prepared BG reveals cubic morphology with even distribution. The sample BG600 has similar morphology with increased particle size. Upon increasing the temperature to 700 °C the particle tend to agglomerate into need-like crystalline state of large particles. Furthermore, these needle particles undergo agglomeration to exhibit flake-like morphology when the temperature was raised to 800 °C, which can be clearly seen from Fig. 4d. Thus, the variation of average particle diameter and length of the samples calculated using ImageJ software are tabulated in Table 3.

3.5. Vickers hardness and apparent porosity

Mechanical properties were analysed using Vickers hardness (HV). The load of 0.98 N was used to indent the bioglass samples and estimate mechanical strength (carried out in triplicates). All BG samples exhibited considerable hardness, of which BG700 expressed higher stability (Table 4). Hardness of BG600 is ~522.7 MPa. BG700 showed higher mechanical strength of ~558 MPa due to higher crystallinity. Subsequently when the temperature was raised to 800 °C, hardness was found to decrease to ~416.8 MPa in BG800. The reduced stability in BG800 may be collectively due to the decomposition of bioglass into another

phase as well as the influence of grain size on hardness [44] according to Hall-Petch theory, which specifies that increasing calcination temperature leads to the rise in the grain size. When grain size reaches the specific limit, grain boundaries start to slide, thus reducing the micro hardness of the material.

Apparent porosity estimated by Archimedes method is shown in Table 4. Maximum porosity of 56% was observed in BG600 that may be due to the spherical

Table 3. Particle size distribution

Samples	Diameter [nm]	Length [nm]
BG as-prepared	429.15	688.63
BG600	947.16	1153.3
BG700	269.36	1452.3
BG800	587.23	1892.9

Table 4. Vickers hardness and apparent porosity estimation

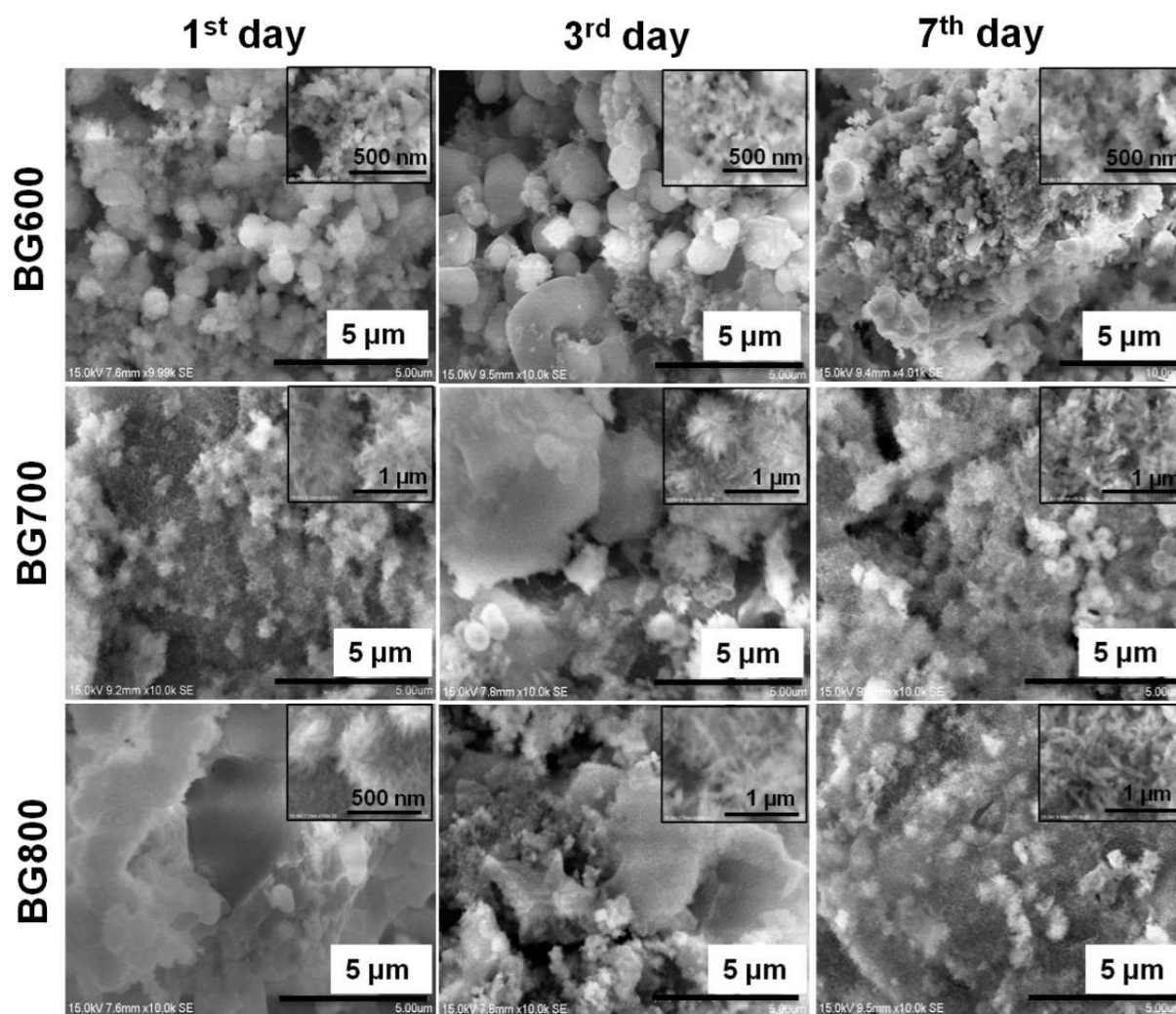| Samples	Vickers hardness		Porosity [%]
	HV	[MPa]	
BG600	53.3 ± 10.7	~522.7	56
BG700	56.9 ± 1.3	~558	20
BG800	42.5 ± 3.6	~416.8	19
BG as-prepared	-	-	41

Figure 5. Morphology of bioglass samples analysed using FESEM after mineralization study

morphology of the corresponding sample. Furthermore, 41% porosity was observed for as-prepared bioglass and 20% and 19% porosity for BG700 and BG800, respectively. Morphology plays a significant role in porosity, which in turn encourages tissue growth and neovascularization [45]. Hence, the results from these experiments suggest BG600 to be more biocompatible and suitable for bone cell adhesion and growth conditions, hence it prompted us to check further the biocompatibility of these samples.

3.6. Biomineralization studies

The results of *in vitro* mineralisation studies for all BG samples are shown in Fig. 5. In all samples morphology completely varies from the first day to the seventh day, which is characteristic for apatite. Compared to BG600 and BG700, the surface changes were promptly observed in BG800 that may be attributed to $Na_2Ca_4(PO_4)_2SiO_4$ crystalline phase. Furthermore it is evident that before immersion all BG samples possess a smooth surface and it is only after the contact with ionic fluid that FESEM micrographs reveal the formation of small apatite-like crystals, which ascertain the forma-

tion of apatite layer. Kokubo *et al.* [46] reported that a calcium phosphate film and SiO_2 rich layer form on the surface of the BG when implanted in the human biological atmosphere that permit bonding towards existing bone. Morphological variations were observed after soaking the samples in SBF. The surface transforms towards apatite formation that were clearly observed after 1, 3 and 7 days of immersion as represented in Fig. 5. After one day of immersion, small particles growth indicates initial period of the growth with spike like apatite on the surface. Moreover, on day three immersed sample showed spindle like projections of calcium phosphate on their surface. A flower-like morphology was observed on the seventh day of immersion, which indicates that calcium phosphate has been deposited on the surface.

3.7. Haemocompatibility studies

Haemolytic activity determines the haemoglobin discharge under the static circumstances [47]. Erythrocyte compatibility is one of the influential factors to investigate the biocompatibility. A compatible result was obtained from the haemolytic assay, all BG sam-
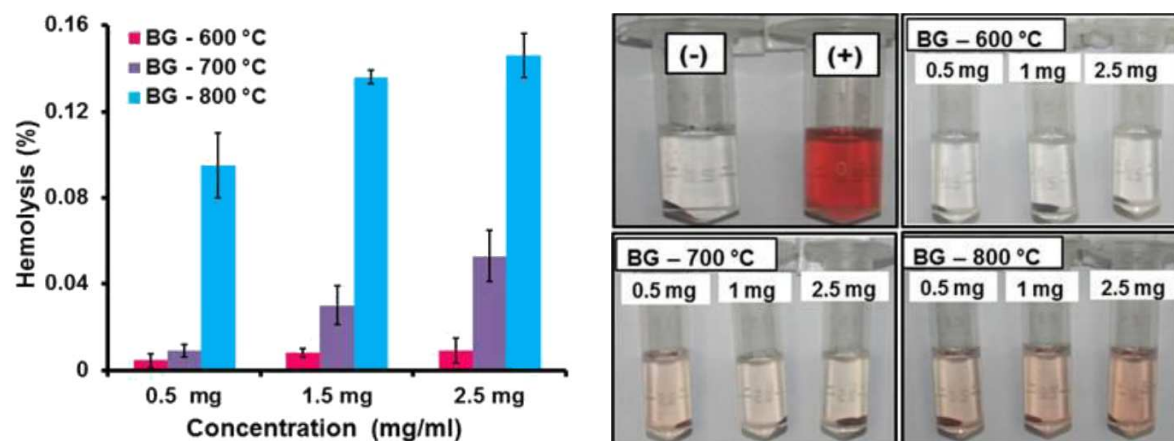
Figure 6. Haemocompatibility assay of BG600, BG700 and BG800 samples

ples showed maximum lysis of 0.15% at a maximum concentration of 2.5 mg/ml. All results were fitted with standard deviation (SD) and the results were considered as statistically significant. As per ASTM standard - F756 (Standard Practice for Assessment of Hemolytic Properties of Materials) below 2% is non-haemolytic, 2 to 5% is slightly haemolytic and above 5% is haemolytic. Figure 6 shows that compared to BG600 and BG700, a slight increase in lysis was noted for BG800 that might be due to the presence of sodium crystals in BG network. Furthermore, higher peak broadening was noted in Raman spectra after immersion, reiterating the increased sodium level in BG700 and BG800. Naturally, sodium crystals have a tendency to damage red blood cells (RBCs) [48]. In the present study, we speculate that with increased sintering temperature, sodium might easily leach out from BG network resulting in lysis of RBCs. Chen *et al.* [49] and Romeis *et al.* [50] reported that increasing sintering temperature attributes to the increased mechanical stability but compromises the biocompatibility. Also, particle size and shape plays a role in biocompatibility [51]. In this study rod-like morphology with micron sized particles were confirmed through FESEM in BG700 and BG800. On the other hand cubical morphology was ex-

hibited in BG600 indicating cube/spherical shape to be more compatible with cells than rod-like morphology.

3.8. Cytocompatibility studies

Osteoblast-like cell line MG-63 was used to investigate the biocompatibility of BG samples with bone like cells. MTT reduction shows the metabolically active cells in the culture plate. The BG samples were incubated in the culture plates for 24, 48 and 72 h duration (Fig. 7). Gradual increase in proliferation rate was observed from the first day onwards. Overall BG samples showed a maximum of 94.34% and a minimum of 88.25% cell viability with the concentration level of 50 μg/ml. BG600 shows 92.86% cell viability in 24 h. In the case of 48 h it is 93.84% and for 72 h it increased up to 94.34% of proliferation. Similarly, BG700 shows the viability of 92.4% in 24 h, 90.74% in 48 h and 91.04% in 72 h. Furthermore, 88.25% viability was noted in 24 h, 85.53% in 48 h and 90.63% in 72 h for BG800. Compared to BG800 better compatibility was achieved for BG600. BG600 incubated cells showed gradual proliferation from 24 to 72 h but in BG700 and BG800 proliferation rate was reduced on the second day and then increased on the third day that could not be explained from the data in the present study. Increasing the sin-
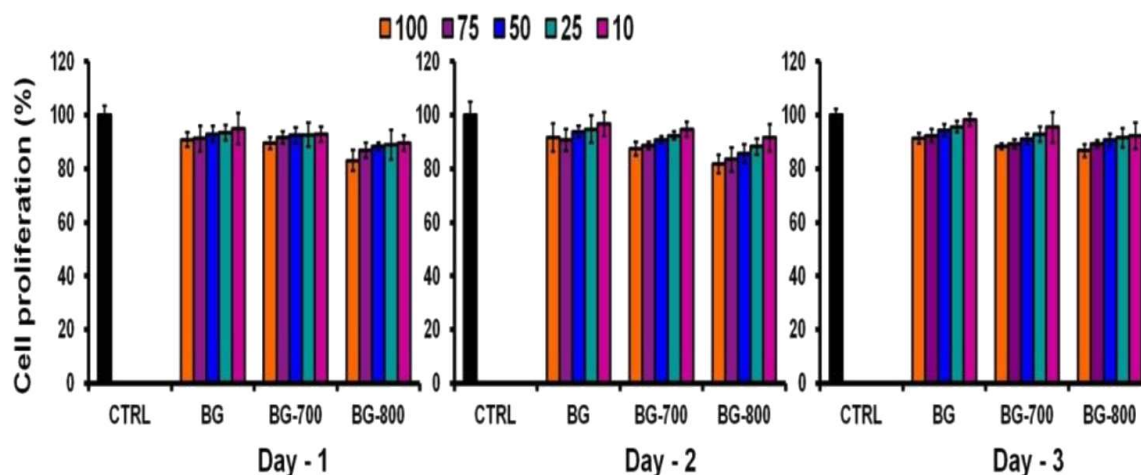

Figure 7. Cytocompatibility studies shows the cell viability and proliferation percentage of bioglass samples

tering temperature reduces biocompatibility, which was found to be consistent with haemocompatibility assay, yet it should be noted that the level of lysis was still within the recommendation of international standards. Nevertheless, relative proliferation of MG-63 cell line on BG600 was found to be higher than BG700 and BG800.

Micrographs of the MG-63 cell line are displayed in Fig. 8 showing proliferation of MG-63 with BG samples. Cells were incubated from 24 up to 72 h with BG samples (concentration 50 μg/μl) sintered at various temperatures. The optical microscope images show gradual growth compared to control. All the samples supported cell viability. Biocompatibility of BG600 showed better results than BG800 because BG600 has combite mineral phase ($Na_2Ca_2Si_3O_9$) that enhanced the biocompatibility and also showed semi-crystalline nature. Hence, the amorphous materials interaction with body fluid is better than with crystalline material, so amorphous material facilitates the biocompatibility. From our study, we suggest that BG sintered at 600 °C will be suitable for bone regeneration application. Above this temperature there will be a compromise in bioactivity.

Erythrocyte compatibility of BG600, BG700 and BG800 is represented in the schematic diagram in Fig. 9. BG600 and BG700 have orthorhombic and hexagonal crystal system with $Na_2Ca_3Si_6O_{16}$ and $Na_2Ca_2Si_3O_9$ crystalline phases. Similarly BG800 possesses hexagonal and anorthic crystal system with $Na_2Ca_2Si_3O_9$ and $Na_2Ca_4(PO_4)_2SiO_4$ crystalline phases. Thus, depending on the sintering temperature varied crystalline phases vary and morphologies such as cubes (600 °C) rods (700 °C) and flakes (800 °C) were attained. BG700 and BG800 samples showed slight damage on the erythro-

cyte membrane; therefore comparatively higher lysis percentage was obtained by haemocompatability assay. Altogether BG600 showed elevated compatibility compared to BG700 and BG800.

Previous reports on the glass crystallization mechanism demonstrate that at the first stage glass transition is acquired around 550 °C, followed by separation of glass in-glass-phase around 570 °C. Further increase in sintering temperature induces that glasses possibly lose their homogeneity, resulting in two dissimilar immiscible phases [30]. Accordingly in our case, we gained dual phases $Na_2Ca_3Si_6O_{16}$ and $Na_2Ca_2Si_3O_9$ (BG600 and BG700) and $Na_2Ca_2Si_3O_9$ and $Na_2Ca_4(PO_4)_2SiO_4$ (BG800) in all three bioglass samples. Also, the above phase transitions are accompanied by growth in particle size while the sintering temperature is increased.

The study reveals that BG800 is 90.63% biocompatible and with ~416.18 MPa hardness. Increased bioactivity can be clearly seen from mineralization results. In BG700 hydroxyapatite phase 91.04% biocompatibility and the hardness of ~558 MPa were achieved. Similarly, BG600 exhibits wollastonite along with hydroxyapatite phase due to the mineralization and 94.34% biocompatibility with hardness of about ~522.7 MPa. From the obtained results it is found that mechanical strength enhances up to 700 °C after which it decreases drastically at 800 °C, the reason being that as temperature increases the grain boundaries start to slide thus reducing the micro hardness. BG700 optimally balances the mechanical strength and biocompatibility due to the crystal structure ($Na_2Ca_3Si_6O_{16}$ and $Na_2Ca_2Si_3O_9$) with better crystallinity. Similarly, owing to the amorphous nature, BG600 showed higher compatibility and comparatively acceptable mechanical property. From these results it is concluded that BG600 exhibits better biocompatibility
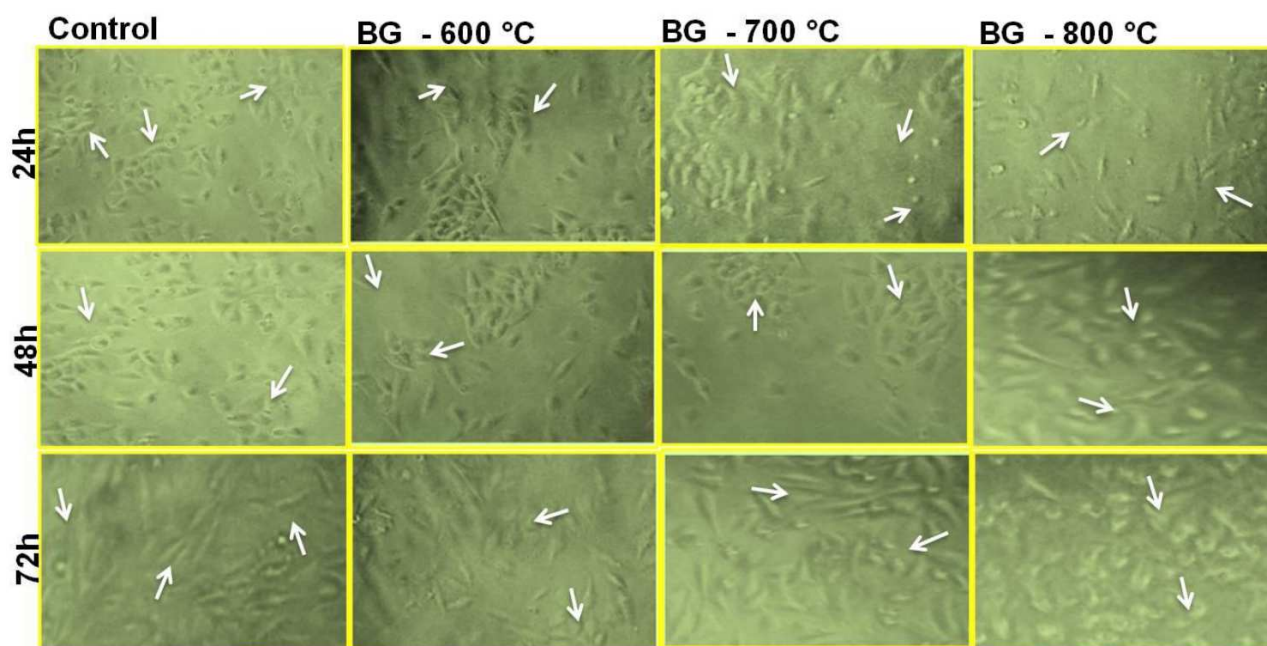

Figure 8. Micrograph of MG-63 cell proliferation after 24, 48 and 72 h observed through microscope (magnification 10×)
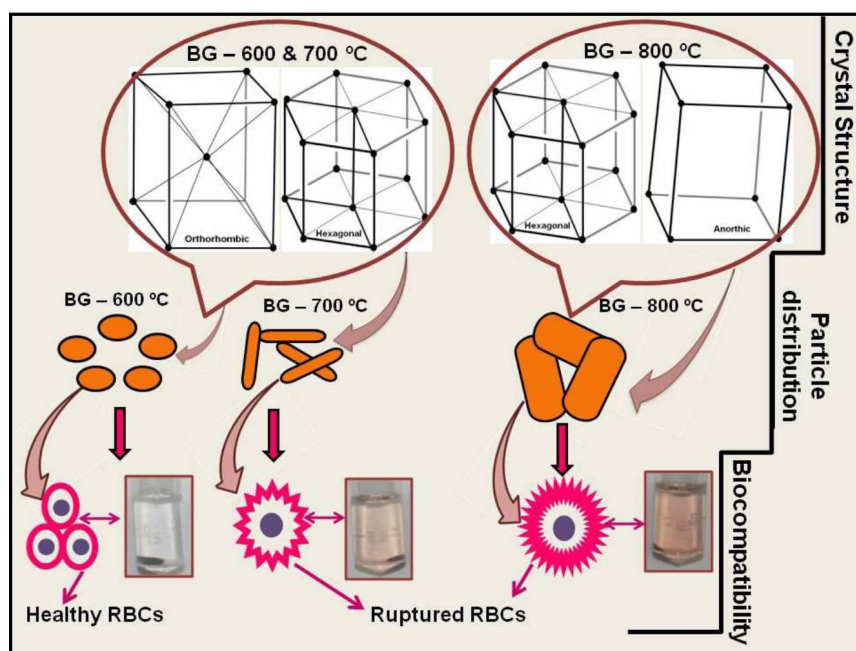
Figure 9. Schematic diagram illustrates the biocompatibility of erythrocytes with bioglass samples

and BG700 exhibits optimal compatibility with higher mechanical stability. Hence we propose that a better compromise in biocompatibility and mechanical stability can be expected for highly efficient bioactive glasses when samples are prepared between 600 and 700 °C.

IV. Conclusions

In the present study, bioglass (BG) was prepared using the sol-gel method and sintered at three different temperatures 600, 700 and 800 °C. It was intended to find the crystallization of BG with respect to the sintering temperature and its influence on the bioactivity and biocompatibility. The crystallization of BG was analysed with XRD. Samples BG600 and BG700 show mixed mineral phases $Na_2Ca_3Si_6O_{16}$ and $Na_2Ca_2Si_3O_9$. Also for sample BG800, $Na_2Ca_2Si_3O_9$ and $Na_2Ca_4(PO_4)_2SiO_4$ dual phases were formed. BG700 showed higher mechanical stability (~558 MPa) because of high crystalline nature and BG600 exhibits improved porosity of 56% and comparatively acceptable mechanical strength of ~522.7 MPa, which might initiate the compatibility with erythrocytes and MG-63 cell lines. *In vitro* immersion studies indicate more rapid hydroxyapatite formation in BG800 and BG700 compared to BG600, which depends on crystallization. In contrast, BG600 expressed higher haemocompatibility rate than BG700 and BG800. Also, compared to BG700 and BG800, acceptable cytocompatibility was obtained for BG600. From this study, it is concluded that 600 and 700 °C calcined bioglasses have possible features to initiate better osteointegration and bone cell proliferation. Thus, we propose that BG600 will optimally initiate osteocytes proliferation and enrich the bone regeneration and BG700 will possibly maintain the mechanical stability. Gene expression and *in vivo* studies will pro-

vide better proof for further validation. From the present study, we also conclude that even though a material may show optimal biomineralization capacity, its biocompatibility may not be optimal. As a result, for a biomaterial to be recommended as a bone substitute, it should be characterised with haemocompatibility, cytocompatibility and ALP activity to understand biocompatibility of the material. Ultimately, this study also proposes that while processing BG for various applications, temperature has to be considered as a vital parameter as it affects bioactivity and compatibility.

References

1. Z. Qiu, H Yang, J Wu, L Wei and J Li, "Ionic dissolution products of NavaBone® promote osteoblastic proliferation via influences on the cell cycle", *J. Int. Med. Res.*, **37** (2009) 737–745.
2. L.L. Hench, "The story of Bioglass®", *J. Mater. Sci: Mater. Med.*, **17** (2006) 967–978.
3. A. Pantchev, E. Nohlert, A. Tegelberg, "Endodontic surgery with and without inserts of bioactive glass PerioGlas® a clinical and radiographic follow-up", *Oral Maxillofac. Surg.*, **13** (2009) 21–26.
4. J.R. Jones, D.S. Brauer, L. Hupa, D.C. Greenspan, "Bioglass and bioactive glasses and their impact on healthcare", *Int. J. Appl. Glass Sci.*, **7** [4] (2016) 423–434.
5. M. Tavakoli, E. Bateni, M. Rismanchian, M. Fathi, A. Doostmohammadi, A. Rabiei, H. Sadeghi, M. Etebari, M. Mirian, "Genotoxicity effects of nano bioactive glass and Novabone bioglass on gingival fibroblasts using single cell gel electrophoresis (comet assay): An in vitro study", *Dent. Res. J.*, **9** [3] (2012) 314–320.

6. J.R. Jones, "Review of bioactive glass from Hench to hybrids", *Acta Biomater.*, **9** (2013) 4457-4486.

7. S. Kumar Nandi, B. Kundu, S. Datta, "Development and applications of varieties of bioactive glass compositions in dental surgery - Third generation tissue engineering, orthopaedic surgery and as drug delivery system", pp. 69–116 in *Biomaterials Applications for Nanomedicine*, R. Pignatello (Ed.). InTech Open, Croatia 2011.

8. M. Mozafari, "Bioceramics in the realm of history", *Bioceram. Dev. Appl.*, **4** [2] (2014) e106.

9. E.S. Sanzana, M. Navarro, M. Ginebra, J.A. Planell, A.C. Ojeda, H.A. Montecinos, "Role of porosity and pore architecture in the in vivo bone regeneration capacity of biodegradable glass scaffolds", *J. Biomed. Mater. Res. A*, **102** [6] (2014) 1767–1773.

10. R. Ravarian, X. Zhong, M. Barbeck, S. Ghanaati, C.J. Kirkpatrick, C.M. Murphy, A. Schindeler, W. Chrzanowski, F. Dehghani, "Nanoscale chemical interaction enhances the physical properties of Bioglass composites", *ACS Nano*, **7** [10] 2013 8469–8483.

11. H. Pirayesh, J.A. Nychka, "Sol-gel synthesis of bioactive glass-ceramic 45S5 and its in vitro dissolution and mineralization behaviour", *J. Am. Ceram. Soc.*, **96** (2013) 1643–1650.

12. D. Durgalakshmi, S.P. Subhathirai, S. Balakumar, "Nanobioglass: A versatile antidote for bone tissue engineering problems", *Procedia Engineer.*, **92** (2014) 2–8.

13. I.D. Thompson, L.L. Hench, "Mechanical properties of bioactive glasses, glass-ceramics and composites", *J. Eng. Med.*, **212** (1998) 127–136.

14. J. Massera, S. Fagerlund, L. Hupa, M. Hupa, "Crystallization mechanism of the bioactive glasses 45S5 and S53P4", *J. Am. Ceram. Soc.*, **95** (2012) 607–613.

15. A. Thomas, J. Bera, "Crystallization and sintering behavior of glass-ceramic powder synthesized by sol-gel process", *J. Austral. Ceram. Soc.*, **52** (2016) 87–91.

16. A.R. Boccaccini, Q. Chen, L. Lefebvre, L. Gremillard, J. Chevalier, "Sintering, crystallisation and biodegradation behaviour of Bioglasss-derived glass-ceramics", *Faraday Discuss.*, **136** (2007) 27–44.

17. L. Lefebvre, L. Gremillard, J. Chevalier, R. Zenati, D. Bernache-Assolant, "Sintering behaviour of 45S5 bioactive glass", *Acta Biomater.*, **4** (2008) 1894–1903.

18. O. Bretcanu, X. Chatzistavrou, K. Paraskevopoulos, R. Conradt, I. Thompsond, A.R. Boccaccini, "Sintering and crystallisation of 45S5 Bioglass® powder", *J. Eur. Ceram. Soc.*, **29** (2009) 3299–3306.

19. B. Lei, X. Chen, Y. Wang, N. Zhao, C. Du, L. Fang, "Influence of sintering temperature on pore structure and apatite formation of a sol-gel-derived bioactive glass", *J. Am. Ceram. Soc.*, **93** [1] 2010 32–35.

20. R. Xin, Q. Zhang, J. Gao, "Identification of the wollastonite phase in sintered 45S5 Bioglass and its effect on in vitro bioactivity", *J. Non-Cryst. Solids*, **356** (2010) 1180–1184.

21. I. Cacciotti, M. Lombardi, A. Bianco, A. Ravaglioli, L. Montanaro, "Sol-gel derived 45S5 Bioglass: Synthesis, microstructural evolution and thermal behaviour", *J. Mater. Sci: Mater. Med.*, **23** (2012) 1849–1866.

22. S. Grasso, R.K. Chinnam, H. Porwal, A.R. Boccaccini, M.J. Reece, "Low temperature spark plasma sintering of 45S5 Bioglass®", *J. Non-Cryst. Solids*, **362** (2013) 25–29.

23. Z. Li, B.C. Thompson, H. Hu, K.A. Khor, "Rapid fabrication of dense 45S5 Bioglass R compacts through spark plasma sintering and evaluation of their in vitro biological properties", *Biomed. Mater.*, **11** (2016) 065006.

24. S. Seyedmajidi, S. Seyedmajidi, H. Alaghehmand, K. Hajian-Tilaki, S. Haghanifar, E. Zabihi, R. Rajabnia, M. Seyedmajidi, "Synthesis and characterization of hydroxyapatite/bioactive glass nanocomposite foam and fluorapatite/bioactive glass nanocomposite foam by gel casting method as cell scaffold for bone tissue", *Eurasian J. Analyt. Chem.*, **13** [2] (2018) 1306–3057.

25. A. Kumar, S. Murugavel, A. Aditya, A.R. Boccaccini, "Mesoporous 45S5 bioactive glass: Synthesis, in vitro dissolution and biomineralization behaviour", *J. Mater. Chem. B*, **5** (2017) 8786–8798.

26. D. Durgalakshmi, S. Balakumar, "Analysis of solvent induced porous PMMA-Bioglass monoliths by the phase separation method – Mechanical and in vitro biocompatible studies", *Phys. Chem. Chem. Phys.*, **17** (2015) 1247–1256.

27. A.M. El-Kady, M.M. Farag, "Bioactive glass nanoparticles as a new delivery system for sustained 5-fluorouracil release: Characterization and evaluation of drug release mechanism", *J. Nanomater.*, **2015** (2015) 839207.

28. D. Bellucci, V. Cannillo, A. Sola, "An overview of the effects of thermal processing on bioactive glasses", *Sci. Sinter.*, **42** (2010) 307–320.

29. C. Ashok Raja, S. Balakumar, D. Durgalakshmi, R.P. George, B. Anandkumar, U. Kamachi Mudali, "Reduced graphene oxide/nano-Bioglass composites: Processing and super-anion oxide evaluation", *RSC Adv.*, **6** (2016) 19657.

30. L. Lefebvre, J. Chevalier, L. Gremillard, R. Zenati, G. Thollet, D. Bernache-Assollant, A. Govin, "Structural transformations of bioactive glass 45S5 next term with thermal treatments", *Acta Mater.*, **55** [10] (2007) 3305–3313.

31. I. Notingher, J.R. Jones, S. Verrier, I. Bisson, P. Embanga, P. Edwards, J.M. Polak, L.L. Hench, "Application of FTIR and Raman spectroscopy to characterisation of bioactive materials and living cells", *Spectroscopy*, **17** (2003) 275–288.

32. V. Maquet, A.R. Boccaccini, L. Pravata, I. Notingher, R. Jerome, "Porous poly (α-hydroxyacid)/bioglass composite scaffolds for bone tissue engineering. Preparation and in vitro characterization", *Biomaterials*, **25** (2004) 4185–4194.

33. H. Aguiar, J. Serra, P. Gonzalez, B. Leon, "Structural study of sol-gel silicate glasses by IR and Raman spectroscopies", *J. Non-Cryst. Solids*, **355** (2009) 475–480.

34. A. Balamurugan, G. Sockalingum, J. Michel, J. Faure, V. Banchet, L. Wortham, S. Bouthors, D. Laurent-Maquin , G. Balossier, "Synthesis and characterisation of sol gel derived bioactive glass for biomedical applications", *Mater. Lett.*, **60** (2006) 3752–3757.

35. L. Marsich, L. Moimas, V. Sergo, C. Schmid, "Raman spectroscopic study of bioactive silica-based glasses: The role of the alkali/alkali earth ratio on the non-bridging oxygen/mridging oxygen (NBO/BO) ratio", *Spectroscopy*, **23** (2009) 227–232.

36. J. Kwiatkowska, K. Suchanek, B. Rajchel, "Bioactive glass coatings synthesized by pulsed laser deposition technique", *Acta Phys. Polonica A*, **211** (2012) 502–505.

37. O. Peitlfilho, G.P. Latorre, L.L. Hench, "Effect of crys-

tallization on apatite-layer formation of bioactive glass 45S5", *J. Biomed. Mater. Res.*, **30** (1996) 509–514.

38. G.A. Stanciu, I. Sandulescu, B. Savu, S.G. Stanciu, K.M. Paraskevopoulos, X. Chatzistavrou, E. Kontonasaki, P. Koidis, "Investigation of the hydroxyapatite growth on bioactive glass surface", *J. Biomed. Pharmac. Eng.*, **1** [1] (2007) 34–39.

39. G. Theodorou, O.M. Goudouri, E. Kontonasaki, X. Chatzistavrou, L. Papadopoulou, N. Kantiranis, K.M. Paraskevopoulos, "Comparative bioactivity study of 45S5 and 58S Bioglasses in organic and inorganic environment", *Bioceram. Develop. Appl.*, **1** (2011) D110154.

40. I. Rehman, W. Bonfield, "Characterization of hydroxyapatite and carbonated apatite by photo acoustic FTIR spectroscopy", *J. Mater. Sci: Mater. Med.*, **8** (1997) 1–4.

41. J. Serra, P. Gonzalez, S. Liste, C. Serra, S. Chiussi, B. Leon, M. Perez-Amor, H.O. Yeanen, M. Hupa, "FTIR and XPS studies of bioactive silica based glasses", *J. Non-Cryst. Solids*, **332** (2003) 20–27.

42. A. Vulpoi, L. Baia, S. Simon, V. Simon, "Silver effect on the structure of SiO_2-CaO-P_2O_5 ternary system", *Mater. Sci. Eng. C*, **32** (2012) 178–183.

43. V.K. Vyas, A.S. Kumar, A. Ali, S. Prasad, P. Srivastava, S.P. Mallick, M. Ershad, S.P. Singh, R. Pyare, "Assessment of nickel oxide substituted bioactive glass-ceramic on in vitro bioactivity and mechanical properties", *Bol. Soc. Esp. Ceram. V.*, **55** (2016) 228–238.

44. K.A. Khalil, S.W. Kima, H.Y. Kimb, "Consolidation and mechanical properties of nanostructured hydroxyapatite-(ZrO_2 + 3 mol% Y_2O_3) bioceramics by high-frequency induction heat sintering", *Mater. Sci. Eng. A*, **456** (2007) 368–372.

45. B. Feng, Z. Jinkang, W. Zhen, L. Jianxi, C. Jiang, L. Jian, M. Guolin, D. Xin, "The effect of pore size on tissue in growth and neovascularization in porous bioceramics of controlled architecture in vivo", *Biomed. Mater.*, **6** (2011) 015007.

46. T. Kokubo, H. Takadama, "How useful is SBF in predicting in vivo bone bioactivity", *Biomaterials*, **27** (2006) 2907–2915.

47. H. Nan, Y. Ping, C. Xuan, L. Yongxang, Z. Xiaolan, C. Guangjun, Z. Zihong, Z. Feng, C. Yuanru, L. Xianghuai, X. Tingfei, "Blood compatibility of amorphous titanium oxide films synthesized by ion beam enhanced deposition", *Biomaterials*, **19** (1998) 771–776.

48. T. Mocan, "Hemolysis as expression of nanoparticles-induced cytotoxicity in red blood cells", *Biotechn. Molecul. Bio. Nanomedi.*, **1** (2013) 7–12.

49. Q.Z. Chen, J.L. Xu, L.G. Yu, X.Y. Fang, K.A. Khor, "Spark plasma sintering of sol-gel derived 45S5 Bioglass-ceramics: Mechanical properties and biocompatibility evaluation", *Mater. Sci. Eng. C*, **32** (2012) 494–502.

50. S. Romeis, A. Hoppe, R. Detsch, A.R. Boccaccini, J. Schmidt, W. Peukert, "Top-down processing of submicron 45S5 Bioglass for enhanced in vitro bioactivity and biocompatibility", *Procedia Engineer.*, **102** (2015) 534–541.

51. Y. Liu, J. Tan, A. Thomas, D. Ou-Yang, V.R. Muzykantov, "The shape of things to come: importance of design in nanotechnology for drug delivery", *Therap. Deliv.*, **3** [2] (2012) 181–194.